

SPECTRAL UNMIXING OF VEGETATION, SOIL AND DRY CARBON IN ARID REGIONS: COMPARING MULTISPECTRAL AND HYPERSPECTRAL OBSERVATIONS

Gregory P. Asner¹ and Kathleen B. Heidebrecht¹

1. Introduction

Remote sensing of vegetation cover and condition is critically needed to understand the impacts of land use and climate variability in arid and semi-arid regions. However, remote sensing of vegetation change in these environments is difficult for several reasons. First, individual plant canopies are typically small and do not reach the spatial scale of typical Landsat-like satellite image pixels. Second, the phenological status and subsequent dry carbon (or non-photosynthetic) fraction of plant canopies varies dramatically in both space and time throughout arid and semi-arid regions. Detection of only the “green” part of the vegetation using a metric such as the normalized difference vegetation index (NDVI) thus yields limited information on the presence and condition of plants in these ecosystems. Monitoring of both photosynthetic vegetation (PV) and non-photosynthetic vegetation (NPV) is needed to understand a range of ecosystem characteristics including vegetation presence, cover and abundance, physiological and biogeochemical functioning, drought severity, fire fuel load, disturbance events and recovery from disturbance.

Many approaches have been devised to analyze PV, NPV and bare soil cover in arid and semi-arid regions. A wide variety of studies have attempted to correlate vegetation indices (e.g., NDVI) to the fractional coverage of PV and bare soil (e.g., Duncan et al. 1993, Carlson and Ripley 1997). The typical spectral regions used to detect PV – the visible and near-infrared wavelengths (0.4-1.3 μm) – do not easily separate the individual contribution of NPV and bare soil to the measurement (van Leeuwen and Huete 1996, Asner 1998, Roberts et al. 1998, Asner et al. 2000). More recently, spectral mixture analysis (SMA) was developed to decompose image pixels into constituent PV, NPV and bare soil covers. Many SMA efforts have now been applied in arid and semi-arid ecosystems using airborne and spaceborne sensors (e.g., Smith et al. 1990, Sohn and McCoy 1997, Wessman et al. 1997, Elmore et al. 2000). Most SMA approaches assume that image pixels contain endmember cover fractions that are linearly summed:

$$\rho(\lambda)_{\text{pixel}} = \sum [C_e \cdot \rho(\lambda)_e] = [C_{\text{pv}} \cdot \rho(\lambda)_{\text{pv}} + C_{\text{soil}} \cdot \rho(\lambda)_{\text{soil}} + C_{\text{npv}} \cdot \rho(\lambda)_{\text{npv}}] \quad (1)$$

where $\rho(\lambda)_e$ is the reflectance of each land-cover endmember (e) at wavelength λ . The sub-pixel cover fraction (C_e) of each land-cover endmember may be PV, NPV, bare soil or other constituents. Solving for the sub-pixel cover fractions (C_e) therefore requires that the observations (in this case, reflectance or $\rho(\lambda)_{\text{pixel}}$) contain enough information to solve a set of linear equations, each of the form of equation (1) but at a different wavelength (λ).

The selection of reflectance endmembers ($\rho(\lambda)_e$) for equation (1) is also critical to the accurate estimation of the sub-pixel cover fractions (C_e). These endmembers are usually selected either from the image data (e.g., Wessman et al. 1997) or from spectral libraries built from field surveys (e.g., Roberts et al. 1998). Each approach has distinct advantages and disadvantages. Image-based endmembers are ideal because they are drawn from the population of data points to be analyzed, which increases the likelihood that image pixels will be decomposed using endmembers that actually exist in the area. However, selection of image endmembers often requires the availability of pixels comprised purely of each dominant cover type. Pure image pixels are rarely available in images of ecosystems, especially in arid and semi-arid regions. A very unique method for addressing this issue has been developed by Bateson and Curtiss (1996) and Bateson et al. (2000). Nonetheless, no automated, fully objective methods have been developed for dealing with sub-pixel heterogeneity in image endmember selection.

The alternative approach of spectral endmember libraries has its advantages and problems as well. The major advantages are that endmembers can be readily collected from large field-based surveys and that the quality and interpretation of the endmembers are easy to control. The potential problems in using spectral libraries relate to endmember generality and scalability. Spectral endmembers collected in one area may not be applicable to another

¹ Carnegie Institution, Stanford, California, 94305.

area, depending on the spatial and temporal variability of vegetation, soils, rocks and other features. Equally important, vegetation spectral properties collected at the leaf or branch level, or very close to the top of a plant canopy, usually do not well represent the spectral properties of the entire plant canopy, which includes all of the tissues, their architectural orientation, and within-crown gaps (Asner 1998, Asner in press).

Of the many spectral mixture modeling methods presented in the literature, all have either used multi-spectral or hyperspectral observations to decompose image pixels into constituent endmember cover fractions (C_e of eq. 1). To our knowledge, no studies have objectively compared the capabilities of multi-spectral and hyperspectral observations with spectral mixture analysis to estimate PV, NPV and bare soil extent in arid and semi-arid ecosystems. To do so requires: (1) that the generality and scalability of the endmember spectra are controlled for in the experiment; (2) that the spectral resolution of the endmember spectra and image data are adjusted between multi-spectral and hyperspectral cases in a consistent manner; and (3) that the spectral mixture model is general, fully automatic and thus resistant to subjective decision-making, such as in the determination of spectral endmembers.

In this paper, we present a study that quantitatively compares the ability of various multi-spectral and hyperspectral observations to decompose remotely sensed optical data into sub-pixel photosynthetic vegetation (PV), non-photosynthetic vegetation (NPV) and bare soil covers. We employed five different spectroscopic sampling schemes available from the NASA Airborne Visible-Infrared Imaging Spectrometer (AVIRIS) as well as with these data convolved to Landsat Thematic Mapper (TM), Terra Moderate Resolution Imaging Spectrometer (MODIS), and Terra Advanced Spaceborne Thermal Emission and Reflection Radiometer (ASTER) optical channels. The analysis using the six optical Landsat TM channels was selected to represent one of the most commonly available satellite data sets for land-cover monitoring. The ASTER analysis was selected because of its relatively dense 5-channel sampling of the shortwave-IR2 (SWIR2) region between 2.1 and 2.4 μm . We tested MODIS because it is available on a daily basis, and it provides a 15-channel sampling of the visible and NIR spectral regions.

2. Study Region

The study area was located in the northeast Chihuahuan Desert, New Mexico, USA at the U.S. Department of Agriculture (USDA) Jornada Experimental Range (Figure 1). Mean annual precipitation is 210 mm yr^{-1} , and mean annual temperature is 16°C (min: -7°C, max: 38°C). The area is also a U.S. National Science Foundation (NSF) Long-term Ecological Research (LTER) site, and has been the focus of many hydrologic and ecological studies associated with land use in arid ecosystems (Schlesinger and Pilmanis 1998). Long-term grazing and fire suppression have been factors in the observed conversion of desert grasslands to shrublands (Buffington and Herbel 1965, Schlesinger et al. 1990). Some areas remain dominated by *Bouteloua eriopoda* (black grama) grasslands, while other areas have been transformed into *Prosopis glandulosa* (mesquite) shrublands. The grasslands are also sparsely populated by *Prosopis* shrubs and occasional yucca plants (*Yucca elata*). The shrublands are comprised of a two-phase landscape containing dune-like mesquite clusters imbedded in a bare soil surface.

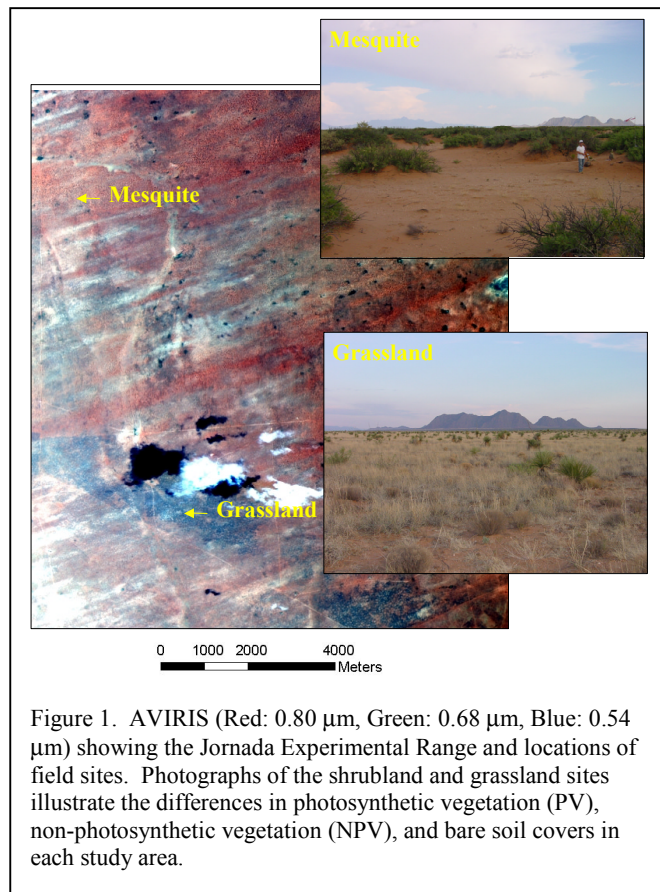


Figure 1. AVIRIS (Red: 0.80 μm , Green: 0.68 μm , Blue: 0.54 μm) showing the Jornada Experimental Range and locations of field sites. Photographs of the shrubland and grassland sites illustrate the differences in photosynthetic vegetation (PV), non-photosynthetic vegetation (NPV), and bare soil covers in each study area.

3. Site Selection and Field Sampling

For this study, the biophysical and geochemical requirements of an experimental grassland and shrubland site included: (1) low species diversity, (2) strong differences in PV cover between sites, (3) pronounced differences in NPV between sites, and (4) nearly constant soil type. These requirements were used to maximize differences in the physical setting between two arid ecosystem sites while minimizing biogeophysical variability within each site. We also selected sites that had few cryptobiotic soil crusts, which can play an important role in determining the “green” reflectance properties of arid ecosystems (Karnieli et al. 1999) and thus confuse our study. Using these requirements, we selected one shrubland and one grassland area, each of 8 ha (200 m x 400 m) in size (Figure 1). A 300 m transect was established in each area running directly north-south (azimuth = 0); geo-location of each transect was achieved using differentially-corrected global position system (GPS) measurements. The following field measurements were made at the two sites in June 2000, coincident with an airborne imaging spectroscopy acquisition using the NASA AVIRIS sensor: (1) species presence-absence, (2) PV, NPV and bare soil cover fraction, and (3) spectroscopy of PV, NPV and bare soil covers.

The vascular plant composition of each site was determined using a presence-absence tabulation of species every 5 m along the 300 m transect. At the grassland site, the fractional cover of PV and NPV was determined using a visible/near-infrared digital camera (Agricultural Digital Camera - ADC; Dycam, Inc.). The camera was mounted 3 m above the ground in the downward nadir-viewing position from a portable boom, yielding an image field-of-view of 1.5 m x 2.5 m. The camera uses visible and near-infrared filters to isolate the fractional cover of PV and bare soil as described by White et al. (2000). Here, we imaged the grassland canopy every 10 m along the centerline of the 300 m transect.

Vegetation cover fraction at the shrubland site could not be adequately determined using the ADC camera because the shrub clusters (~ 5-15 m dia.) are much larger than the field-of-view of the ADC camera (~ 1.5 x 2.5 m). Therefore, we acquired a pan-chromatic IKONOS image with spatial resolution of 1m on July 2, 2000, which was within two weeks of the field sampling and AVIRIS data acquisitions. This imagery was co-located with the AVIRIS data to facilitate comparisons of PV cover along the 300 m transect. Because NPV cover was near zero in the shrubland area, the IKONOS data isolate PV from the soil background.

Canopy and soil spectroscopic measurements were collected using a field spectroradiometer (Fieldspec FR-Pro, Analytical Spectral Devices, Inc.) along each transect in the shrubland and grassland sites and at eight other shrubland and grassland locations throughout the area. The spectroradiometer collects upwelling radiance measurements in the 0.4-2.5 μm wavelength range; the sampling interval is 1.4 μm in the visible and near-IR (0.4-1.0 μm) and 2.0 μm in the shortwave-IR (1.0-2.5 μm). The spectral radiance measurements were collected at 5 m intervals along the 300 m transects and were converted to reflectance using a calibration panel (Spectralon, Labsphere, Inc.). All plant canopies within 5 m radius of the sampling point were measured. At the time of the field survey, the grassland canopies were nearly fully senescent and the shrubland canopies were fully green, allowing us to separate the spectra both by species and by PV-NPV category. In addition, the spectral reflectance properties of bare soil patches were measured at each sampling location along each transect.

4. Airborne Imaging Spectroscopy

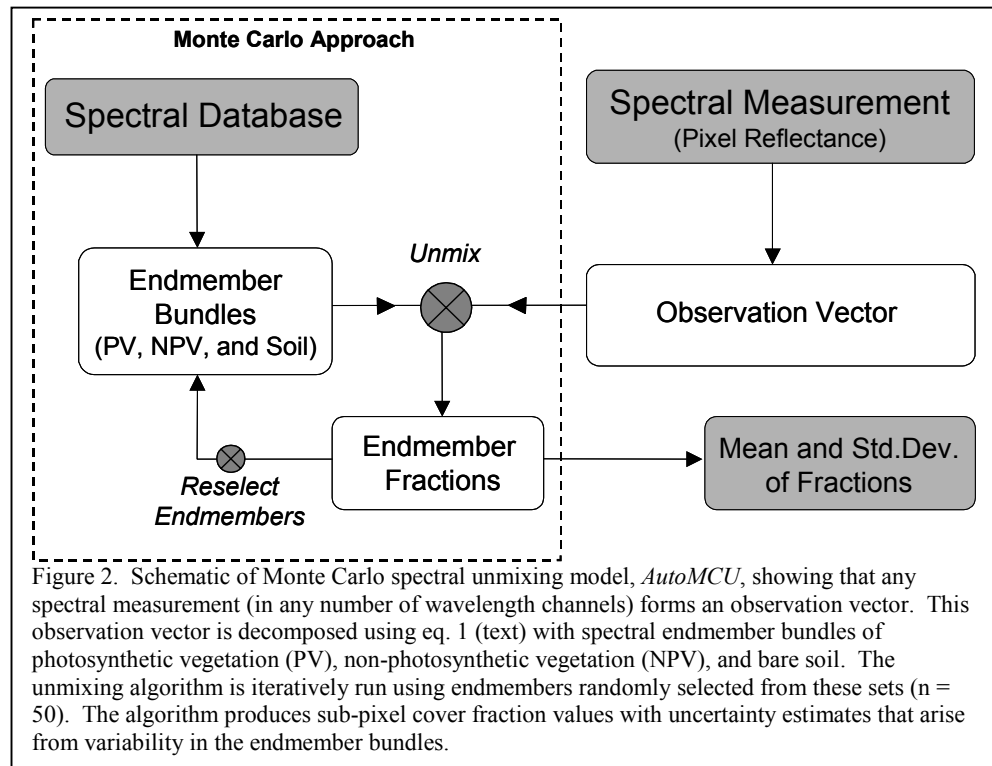
AVIRIS imaging spectroscopy data were collected over the field sites on June 10, 2000, coincident with the field measurement campaign. The AVIRIS sensor was flown on a NASA ER-2 aircraft at an altitude of 20 km, which resulted in image pixels of 19 m x 19 m. The flightlines were oriented in the north-south direction (azimuth = 0°). The imagery was geo-located using roads matched to GPS points in a geographic information system (GIS). The GIS data were provided by the USDA and Jornada LTER staff (courtesy of B. Nolen); the geo-location accuracy of the roads was less than 1 m. The AVIRIS data were converted from radiance to apparent surface reflectance using the ATREM atmospheric calibration code (Gao et al. 1993) and further refined using a field spectral measurement of a bare soil area.

5. Spectral Mixture Analysis

We developed a general, probabilistic model for decomposing optical reflectance measurements into sub-pixel estimates of PV, NPV and bare soil covers. This model is fully automated and uses a Monte Carlo approach to

derive uncertainty estimates of the sub-pixel cover fraction values (Figure 2). The model, *AutoMCU*, is based on a code first developed only for the shortwave-IR spectral region (*AutoSWIR*; Asner and Lobell 2000), but it is more general in that any combination of optical wavelengths can be used in the unmixing process. *AutoMCU* uses three spectral endmember “bundles”, derived from field measurements, to decompose each image pixel using equation (1).

We used the spectra collected in the grassland and shrubland field sites to execute the unmixing code. Our intent was to minimize errors and uncertainty that can arise when unmixing image pixels with spectral endmembers not present in the specific study area. This strategy was critical to comparing the accuracy of sub-pixel cover fraction estimates from different combinations of spectral channels and signature types.



After the three spectral endmember bundles (PV, NPV, soil) were collected from the field, they were subsampled to AVIRIS, Landsat TM, ASTER, and MODIS wavelength channels using published spectral response functions. The AVIRIS imagery was also convolved to the wavelength channels provided by the four satellite instruments. This provided a means to spectrally unmix the same ecological area using the same field spectra and *AutoMCU* code. The only difference between each spectral unmixing was the wavelength sampling. In addition, we tested the accuracy of spectrally decomposing image pixels using only the visible and near-IR (0.4-1.3 μm) and only the shortwave-infrared (SWIR: 1.3-2.5 μm) hyperspectral measurements from AVIRIS.

The SWIR2 (2.0-2.3 μm) spectral unmixing algorithm of Asner and Lobell (2000) was also tested against the other spectral sampling schemes. This algorithm uses SWIR2 spectra that are “tied” at 2.03 μm to isolate the shapes of the PV, NPV and bare soil spectra, which are very distinct in this wavelength region. Based on both field and radiative transfer studies (Asner 1998, Asner et al. 2000), tied-SWIR2 spectra of PV and NPV should be less susceptible to variation in canopy biomass, architecture and leaf biochemistry. Tied-SWIR2 spectral bundles of bare soils accommodate variation in geochemical properties that cause the distinctive 2.2 μm soil hydroxyl (OH) absorption feature to shift in width, shape, and depth (Ben-dor et al. 1999). Therefore by developing bundles of these tied-SWIR2 spectra for use in the Monte Carlo unmixing model, *in situ* variations in biochemical and geochemical properties are propagated to the sub-pixel cover fraction estimates.

Some studies have divided the spectral reflectance values within a given wavelength region by the reflectance value at the first wavelength. This is analogous to tying at 2.03 μm , but dividing is often used to accentuate the distinctive absorption features of various materials (Clark 1999). We therefore also test the spectral unmixing model using divided SWIR2 data. In addition, the SWIR2 data in five ASTER channels provide a means to test both the tying and dividing approaches using an available multi-spectral satellite instrument. This comparison is especially pertinent here since the ASTER and AVIRIS instruments have similar spatial resolutions of

15-30m and ~20m, respectively. All of the spectral wavelength sampling and signature permutations compared in this study are presented in Table 1.

6. Results and Discussion

Species Composition

The vascular plant presence-absence survey yielded the following information verifying that the first criterion for site selection (low plant diversity) was successfully met. At the shrubland site, 98.9% of the species present was *Prosopis glandulosa*, and 1.1% was comprised of small, fully senescent herbaceous grasses and forbs (species undetermined). At the grassland site, the species present were *Bouteloua eriopoda* and other graminoids (99.3% of the time), *Prosopis* (4.7%), and *Yucca* spp. (3.3%).

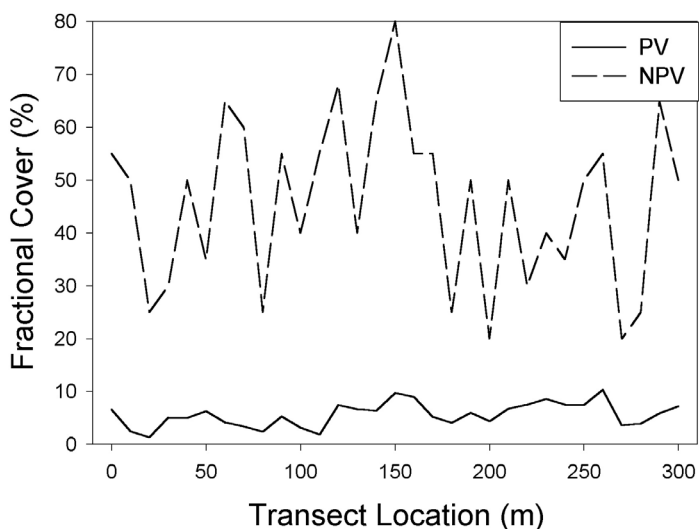


Figure 3. Photosynthetic vegetation (PV) and non-photosynthetic vegetation (NPV) cover along a 300 m transect cutting through the 8 ha grassland study site. PV and NPV fractions were calculated using the method described in detail by White et al. (2000).

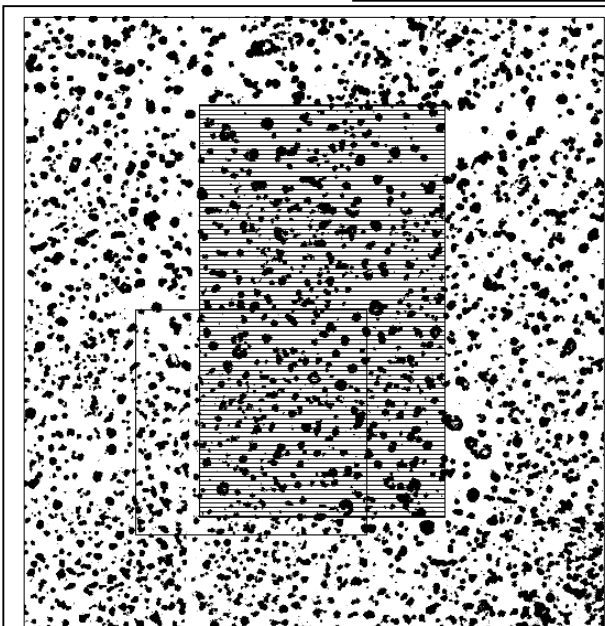


Figure 4. IKONOS image of a 50 ha mesquite (*Prosopis glandulosa*) shrubland area. Large shrub-dunes are visible throughout this region. The rectangular box indicates extent of 200 x 400 m (8 ha) study area, showing the photosynthetic vegetation (PV) cover of 18%. The square box shows the extent and overlap of the 200 x 200 m study area from Rango et al. (2000), which indicated a PV cover of 19%.

PV, NPV and Bare Soil Cover

At the grassland site, the ADC camera results yielded a mean PV cover of 6.9% (std. dev. = 3.3%), with a range of 1% to 18% (Figure 3). Bare soil fraction estimates yielded mean (s.d.) values of 58.6 (17.3) %, with a range of 20% to 80%. Asner et al. (2000) had estimated PV fractional cover of 4-11% along a neighboring grassland transect in May 1997. Those values were determined independently from our values reported here, by measuring total vegetation cover and multiplying it by the NPV:PV ratio of 1m sub-plots in the area.

At the shrubland site, the high spatial resolution IKONOS imagery indicated a PV and bare soil cover fraction of 18% and 82%, respectively, throughout the 8 ha area surrounding our 300m transect (Figure 4). This concurs with recent laser altimetry data that yielded PV and bare soil cover estimates of 19% and 81%, respectively (Rango et al. 2000). These estimates also agree with those reported by Schlesinger et al. (1996) and Asner et al. (2000).

NPV was extremely low (< 2%) at the shrubland site as is evident in our field transect of plant

presence-absence as well as in our visual surveys of the area (Figure 1). NPV was extremely high at the grassland site (mean = 36.7%, s.d. = 13.3%), with values ranging from 10-70% along the 300m transect. These estimates concur with recent studies conducted in the same or similar areas (Schlesinger et al. 1996, Asner et al. 2000).

Field Spectroscopy

Field spectral data collections yielded distinct spectral endmember bundles for PV, NPV and bare soil (Figure 5). The PV spectra from shrubland and grassland sites were not statistically different (t-tests by wavelength), and thus they were combined into a single PV endmember set for all subsequent spectral mixture analyses (Figure 5a). The PV spectra showed typical value ranges for the visible, NIR, and SWIR wavelength regions as found in many arid ecosystems (Asner 1998). The greatest spectral variation occurred in the NIR (0.7-1.3 μm) and was the lowest in the SWIR2 region from 2.1-2.4 μm . The strong NIR spectral variation is indicative of highly varying leaf area index (LAI) at the scale of individual plant canopies (Asner et al. 2000). While the SWIR2 region did show some variability in the magnitude of reflectance, the spectral shapes were highly consistent (Figure 5d).

The NPV spectra were collected only from the grassland site, as very little NPV was present or exposed at the shrubland site. These NPV spectra were used in all mixture modeling analyses of both sites. Consistent with previous studies, the NPV spectra showed almost constant monotonic-increasing reflectance in the visible-NIR region (Figure 5b). Several dry carbon spectral absorption features in the SWIR2 region are clearly apparent. The features near 2.1 and 2.4 μm are associated with the presence of cellulose, starch and oils (Curran 1989). While the magnitude of reflectance varied strongly in the SWIR2 region, the shapes of the spectra were highly consistent (Figure 5e).

The soil spectra were similar between sites (t-tests by wavelength), thus they were combined into a single endmember set for spectral mixture analyses. The well-described OH⁻ absorption feature near 2.2 μm is apparent (Figure 5c), as are the visible wavelength features associated with the presence of iron (Ben-dor et al. 1999). Again, the shapes of the soil spectra in the SWIR2 region were distinct from PV and NPV, and they were relatively consistent (Figure 5f).

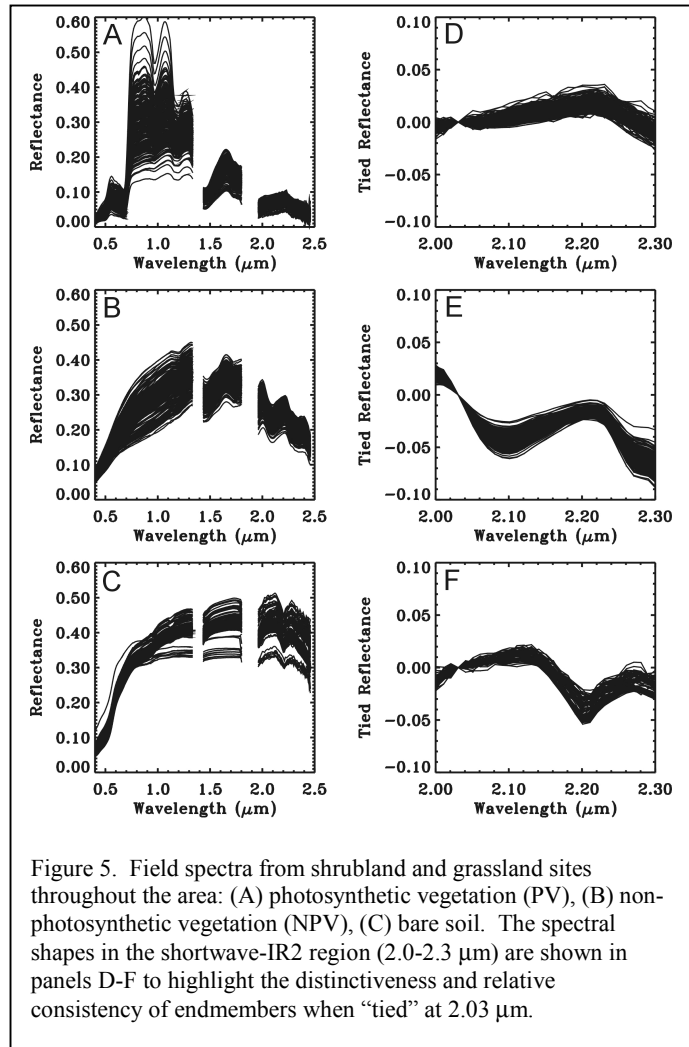


Figure 5. Field spectra from shrubland and grassland sites throughout the area: (A) photosynthetic vegetation (PV), (B) non-photosynthetic vegetation (NPV), (C) bare soil. The spectral shapes in the shortwave-IR2 region (2.0-2.3 μm) are shown in panels D-F to highlight the distinctiveness and relative consistency of endmembers when “tied” at 2.03 μm .

AVIRIS and AVIRIS-Convolved Spectra

The AVIRIS spectra from the shrubland and grassland sites are shown in Figure 6a-b. Subtle differences between sites can be seen in the AVIRIS spectroscopy throughout the visible-NIR transition, the SWIR1 (1.5-1.8 μm) and the SWIR2 (2.0-2.4 μm) wavelength regions. The magnitudes of reflectance values from each site were statistically similar at nearly all wavelengths (t-tests by wavelength). Visual inspections also showed the shapes of the spectra in the visible, NIR and SWIR1 regions to be very similar. However, the shapes of the reflectance continuum in the SWIR2 region were unique between the shrubland and grassland sites (Figure 6c-d). Tied-SWIR2

spectra visually indicate that the shrubland site contained high bare soil cover due to well-defined 2.2 μm OH⁻ absorption features (Figure 6c). The grassland site displayed weaker OH⁻ features in the tied-SWIR2 spectra (Figure 6d). Tied SWIR2 spectra in the 2.02-2.12 μm region from the grassland site indicated the presence of significantly more NPV than in the shrubland site. The convex shapes of the tied-SWIR2 data from the grassland site were distinct from the concave shapes of the data from the shrubland site.

The Landsat TM-convolved data showed little difference between the shrubland and grassland sites (Figure 7a), with only a slight difference in albedo in the NIR and SWIR wavelengths. The MODIS data provided an increased sampling of the visible and NIR spectral regions (Figure 7b), yet the two field sites were spectrally indistinguishable using these channels. This was the case for the visible-NIR channels in the AVIRIS data as well (Figure 6a-b).

Previous studies have shown that bare soil and NPV cannot be easily separated in visible-NIR wavelength channels (Huete 1988, van Leeuwen and Huete 1996, Asner et al. 2000). The ASTER data provided a unique multi-spectral

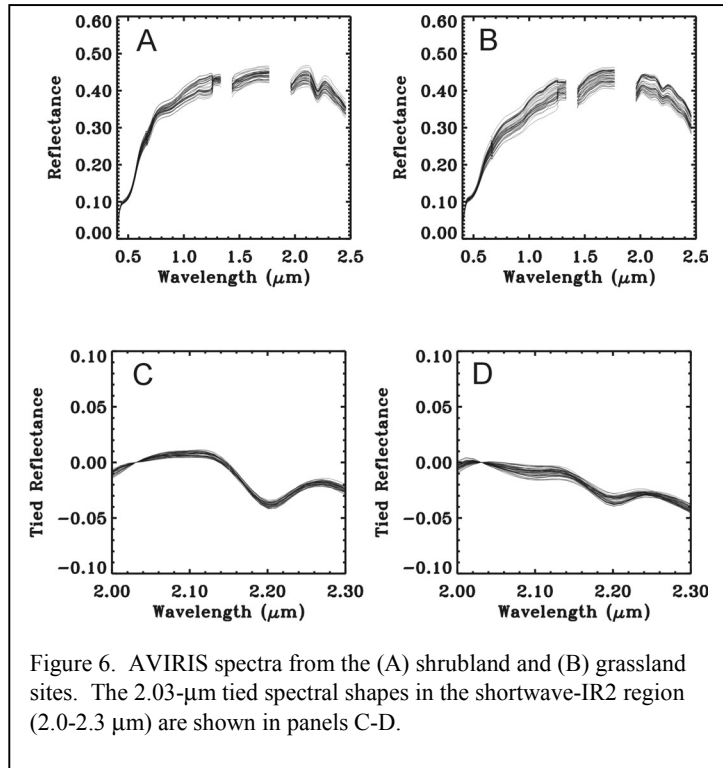


Figure 6. AVIRIS spectra from the (A) shrubland and (B) grassland sites. The 2.03- μm tied spectral shapes in the shortwave-IR2 region (2.0-2.3 μm) are shown in panels C-D.

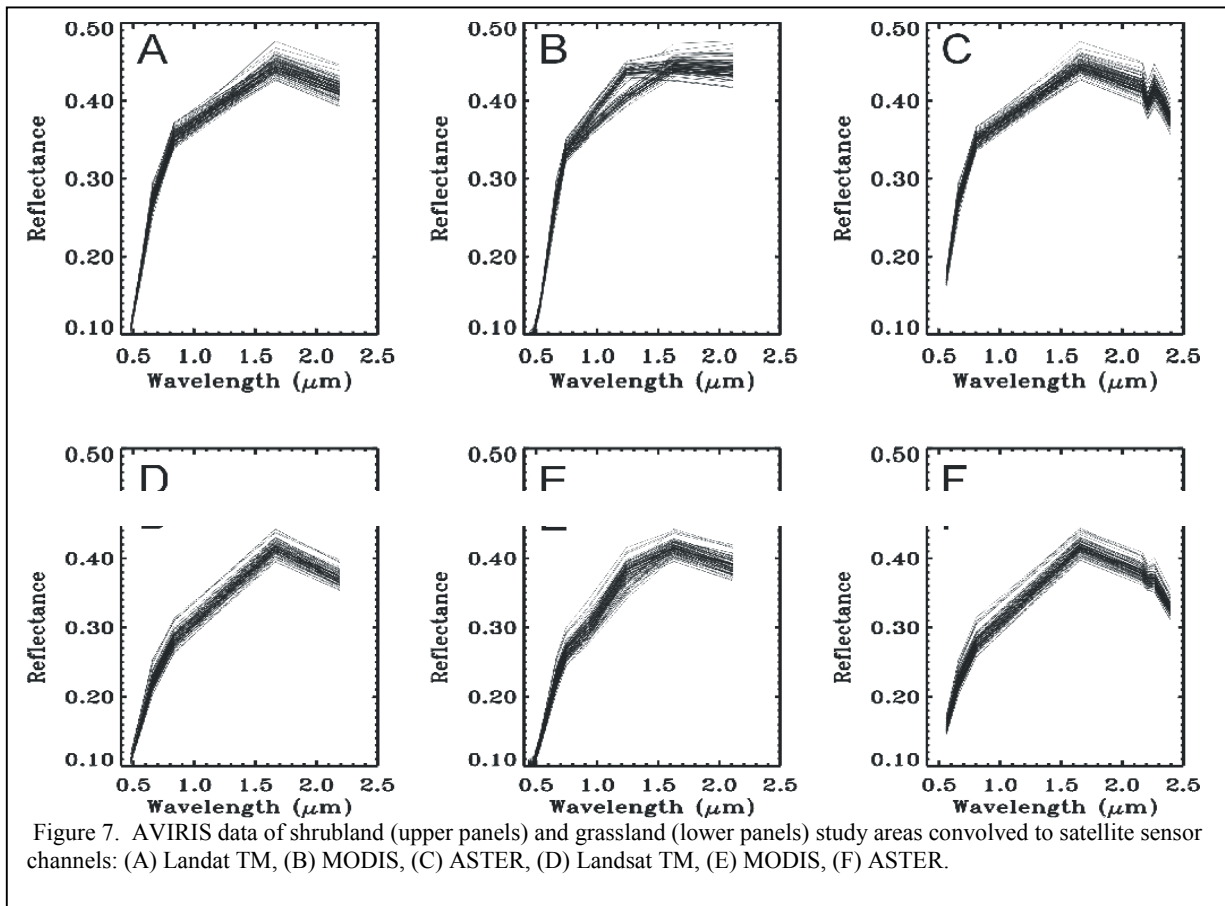


Figure 7. AVIRIS data of shrubland (upper panels) and grassland (lower panels) study areas convolved to satellite sensor channels: (A) Landsat TM, (B) MODIS, (C) ASTER, (D) Landsat TM, (E) MODIS, (F) ASTER.

sampling of the SWIR2 (Figure 7c), indicating some differences between sites. The tied-SWIR2 ASTER data are provided in Figure 8, showing the distinctive OH⁻ absorption feature at 2.2 μm for the shrubland site, and less so for the grassland area. ASTER’s sampling of the SWIR2 region does not resolve the 2.0-2.12 μm wavelengths that are needed for detection of NPV (Figure 5).

Monte Carlo Spectral Mixture Analyses

The Monte Carlo spectral unmixing provided two pieces of information important to this study: (1) the accuracy of PV, NPV, and bare soil estimates and (2) the uncertainty or precision of these estimates. Table 2 shows the spectral decomposition results for the shrubland and grassland sites using the ten different wavelength permutations. The summary of field and IKONOS results are also shown under “Field Measurements” in Table 2.

The full-range AVIRIS unmixing resulted in negative PV fractions, and the bare soil fractions were consistently over-estimated by about 20% (Table 2). However, the estimated NPV fractions were very close to the field NPV values, and within the statistical uncertainty of the two methods (ANOVA, $p < 0.05$). The data show that full spectral range (0.4-2.4 μm) analyses may provide some measure of NPV presence, but they grossly under-estimate PV and over-estimate bare soil extent. These results concur with other studies in arid regions, where very low green vegetation cover and very bright soils often preclude an accurate unmixing of image pixels using full-range AVIRIS data (van Leeuwen et al. 1997, Okin and Roberts 2000). The PV fractions from Monte Carlo unmixing

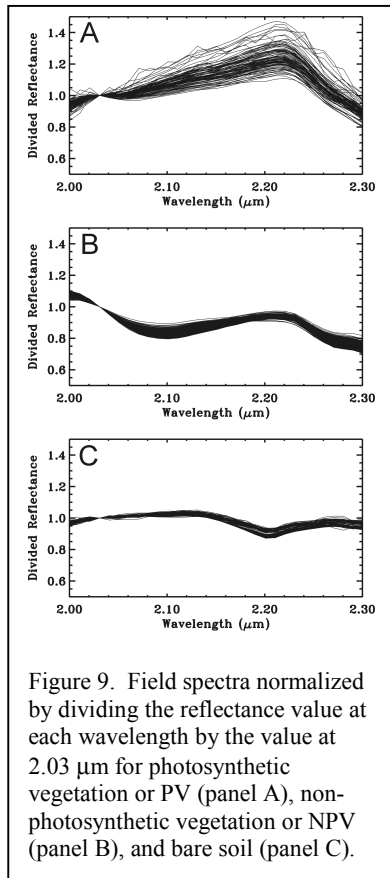


Figure 9. Field spectra normalized by dividing the reflectance value at each wavelength by the value at 2.03 μm for photosynthetic vegetation or PV (panel A), non-photosynthetic vegetation or NPV (panel B), and bare soil (panel C).

were also far under-estimated at both field sites when using only the visible-NIR (VNIR) spectral region (0.4-1.3 μm) of the AVIRIS data (Table 2). This is also likely due to the presence of very bright soil, which saturates this wavelength

region and leads to over-estimates of soil cover. The NPV fraction was also significantly over-estimated using the VNIR-only AVIRIS data. This results from the known confusion when separating NPV and soils using this spectral region (van Leeuwen and Huete 1996, van Leeuwen et al. 1997, Asner et al. 2000).

Spectral unmixing using the un-normalized SWIR2 (2.0-2.3 μm) region of the AVIRIS data yielded similarly poor results that were comparable to the VNIR unmixing (Table 2). In arid and semi-arid regions, SWIR2 spectra are dominated by extremely bright soils and NPV (Figure 5b-c). Like the VNIR, this can lead to a substantial under-estimate of PV cover in these environments.

Spectral unmixing with the “tied” SWIR2 region of the AVIRIS imagery yielded accurate estimates of all three land surface covers (Table 2). The field-measured PV, NPV and bare soil fractions in the shrubland site were well within the statistical uncertainty range of the *AutoMCU* results. While the PV fraction was slightly over-estimated at the grassland site (not statistically significant; ANOVA, $p = 0.09$), both the NPV and bare soil fractions were estimated with high accuracy. These results corroborate the

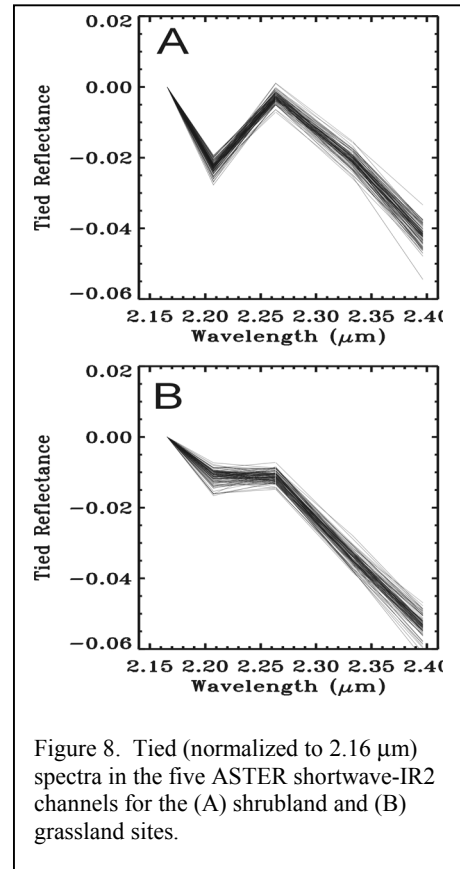


Figure 8. Tied (normalized to 2.16 μm) spectra in the five ASTER shortwave-IR2 channels for the (A) shrubland and (B) grassland sites.

work presented by Asner and Lobell (2000), and indicate that the tied-SWIR2 spectra are a means for estimating the three dominant surface constituents in two dramatically different arid ecosystems.

It is common practice in the spectroscopy community to analyze specific absorption features via spectral normalization by division (Clark 1999). Spectral unmixing with divided-SWIR2 spectra resulted in moderate over-estimates of bare soil extent and major under-estimates of PV (Table 2). The reason for this can be seen in the divided-SWIR2 spectra (Figure 9): normalization by division accentuated the shape of the endmembers relative to the tied-SWIR2 values (Figure 5 d-f). This led to under-estimates of PV and over-estimates of bare soil as the unmixing algorithm attempted to compensate for overly accentuated PV endmembers (Table 2). Moreover, it is mathematically inappropriate to use division-normalized spectra for linear mixture modeling. The diagnostic spectral shapes of each land cover type are exploited by using tied spectra, which remove differences in overall albedo while preserving the linear relation in equation (1). For example, subtracting the reflectance at one wavelength (ρ_0) is valid because a spectrum can still be expressed as the properly weighted sum of endmembers:

$$\begin{aligned}\rho - \rho_0 &= C_{veg} \cdot \rho_{veg} + C_{soil} \cdot \rho_{soil} + C_{litter} \cdot \rho_{litter} - (C_{veg} \cdot \rho_{veg,0} + C_{soil} \cdot \rho_{soil,0} + C_{litter} \cdot \rho_{litter,0}) \\ &= C_{veg} \cdot (\rho_{veg} - \rho_{veg,0}) + C_{soil} \cdot (\rho_{soil} - \rho_{soil,0}) + C_{litter} \cdot (\rho_{litter} - \rho_{litter,0})\end{aligned}\quad (2)$$

However, a nonlinear spectral transformation, such as dividing by ρ_0 , cannot be done within the SMA framework:

$$\frac{\rho}{\rho_0} = \frac{C_{veg} \cdot \rho_{veg} + C_{soil} \cdot \rho_{soil} + C_{litter} \cdot \rho_{litter}}{C_{veg} \cdot \rho_{veg,0} + C_{soil} \cdot \rho_{soil,0} + C_{litter} \cdot \rho_{litter,0}} \neq C_{veg} \frac{\rho_{veg}}{\rho_{veg,0}} + C_{soil} \frac{\rho_{soil}}{\rho_{soil,0}} + C_{litter} \frac{\rho_{litter}}{\rho_{litter,0}}\quad (3)$$

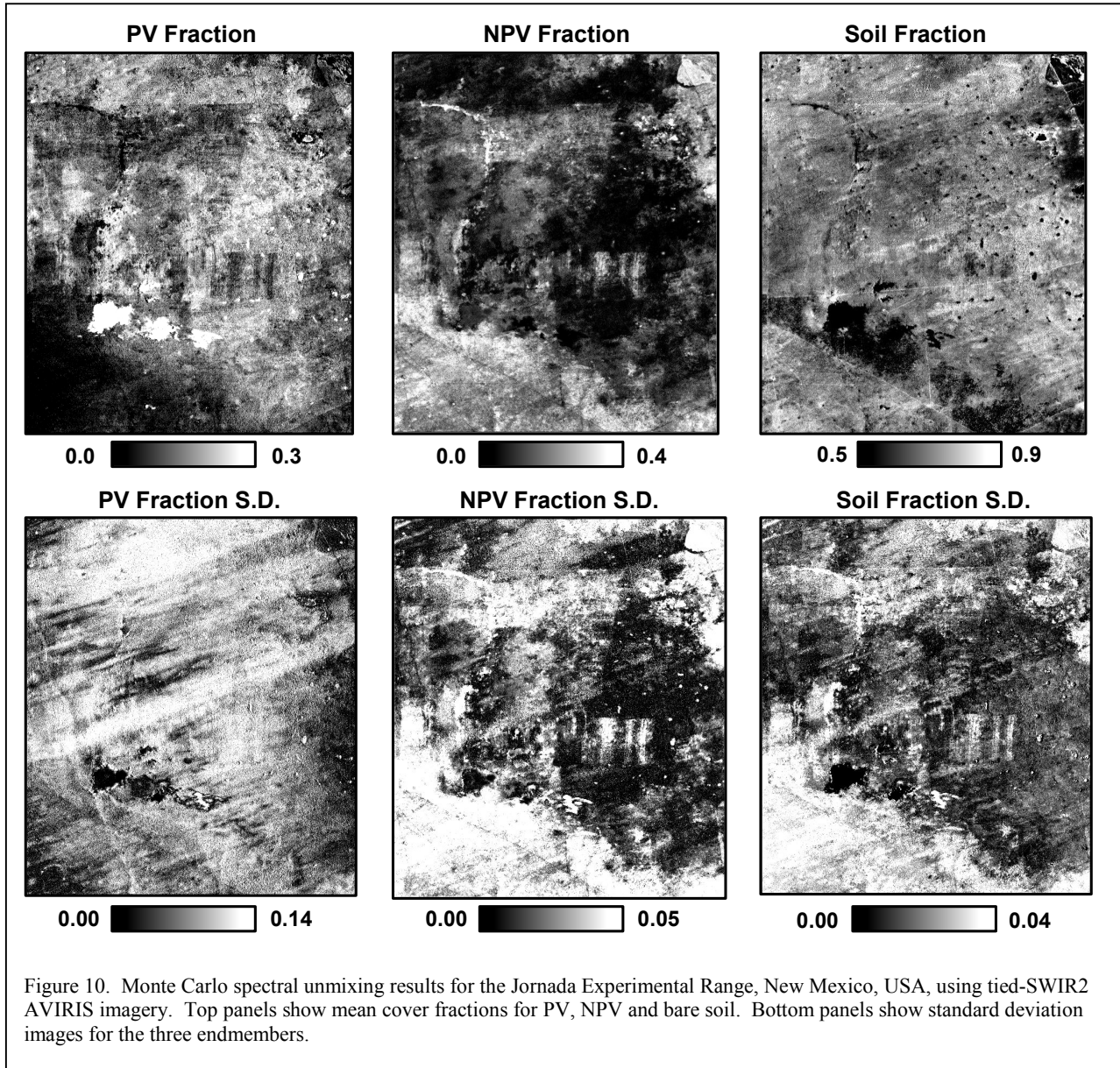
This analysis shows, both mathematically and experimentally, that the use of division-normalized spectra is not appropriate for linear spectral mixture analysis.

The ASTER sensor holds some promise for extending the tied-SWIR2 AVIRIS capability to the multi-spectral spaceborne level, but our results indicated less than ideal estimates of the three cover fractions. The tied-SWIR2 ASTER unmixing did estimate bare soil and PV to within 10% of the field-measured values at the shrubland site (Table 2). However, the NPV fraction was substantially under-estimated at this site. Estimates of bare soil were similarly accurate at the grassland site, while the retrieved PV values were 4-5 times too high and the NPV values were 50% too low. These results can be explained by comparing tied-SWIR2 spectra in AVIRIS (Figure 6c-d) and ASTER (Figure 8a-b) wavelengths. The dense spectral sampling of the 2.0-2.15 μm region by AVIRIS allows for the NPV to be better separated from the bare soil. ASTER's spectral sampling does not begin until 2.16 μm , and thus it does not easily resolve the presence of NPV (only soil via the OH⁻ absorption feature).

Of all wavelength permutations attempted in the Monte Carlo spectral mixture analysis, only the tied-SWIR2 data in AVIRIS channels 2.03-2.30 μm yielded accurate results with low statistical uncertainty (Table 2). The tied-SWIR2 ASTER results showed some promise for estimating bare soil cover; however, additional analysis at more sites is needed to verify the value of ASTER's SWIR2 sampling for this purpose. Based on these findings, the AVIRIS tied-SWIR2 unmixing was extended over the entire Jornada Experimental Range (Figure 10). The shrubland site is located near the western edge of the larger shrubland region, which occupies the upper third of the image. This region has PV cover values ranging from 0-30% and very low NPV cover values of 0-10%. It has very high bare soil cover of greater than 70%. The grassland site is located within a larger black grama grassland in the lower third of these images. This region has very high NPV (>30%), low to moderate PV (0-15%), and relatively low bare soil cover (<60%). The analysis will be extended in future efforts to understand the full variability of vegetation and bare soil extent and its linkages to biogeochemical processes at the regional scale. For now, this study, combined with the study presented by Asner and Lobell (2000), indicates that the tied-SWIR2 spectral mixture analyses using high quality AVIRIS spectroscopic data can be used to estimate the relative and absolute fractional coverages of photosynthetic vegetation, non-photosynthetic vegetation (dry carbon), and bare soil in this arid region.

7. Conclusions

This study considered the accuracy and precision of linear spectral mixture analysis for estimating sub-pixel coverage of photosynthetic vegetation (PV), non-photosynthetic vegetation (NPV), and bare soils in arid regions. The study employed two contrasting arid ecosystems and directly compared a wide variety of spectral sampling schemes in a controlled spectral unmixing or decomposition experiment. This experiment utilized a dense sampling of field spectroscopic endmembers for PV, NPV and bare soil along with a general, probabilistic linear mixture model based on Monte Carlo analysis. Concomitant imaging spectroscopy measurements from the NASA AVIRIS sensor provided a means to test five hyperspectral sampling schemes. The field spectral endmembers and AVIRIS data were also convolved to the optical wavelength channels provided by Landsat TM, MODIS and ASTER.



The comparison indicated clear limitations in using the full optical range (0.4-2.5 μm) or visible-NIR (0.4-1.3 μm) to decompose image pixels into PV, NPV and bare soil covers in an arid shrubland and grassland ecosystem (Table 2). Shortwave-IR2 (SWIR2) measurements in the 2.0-2.3 μm range showed the distinctive differences in PV,

NPV and bare soil spectral properties. When the SWIR2 spectra are normalized by tying each value to that of the first wavelength (2.03 μm), the distinctive shapes of the three endmembers are isolated and the effect of changing albedo is minimized. These tied-SWIR2 endmembers provided verifiably accurate estimates of PV, NPV and bare soil in the shrubland and grassland study areas. No other spectral combination or approach tested in this study could provide similar performance. The tied-SWIR2 sampling provided by ASTER (5 channels; Table 1), provided some useful information on bare soil extent, but poor spectral coverage in the 2.0-2.15 μm range precluded an accurate NPV or a better bare soil estimate.

In general, we believe that the SWIR2 spectral region is one of the best ways to estimate the fractional cover of photosynthetic vegetation, non-photosynthetic vegetation, and bare soils in arid regions. To date, only a few instruments, such as the AVIRIS, provide the SWIR2 spectral sampling with sufficiently high signal-to-noise ratio for use in our Monte Carlo mixture model. Further testing and analysis of the SWIR2 region for analyzing the presence and abundance of these land surface materials will continue in our future efforts. Ecological and biogeochemical research efforts at the landscape and regional scale require detailed information on the spatial and temporal variability of live vegetation, dry carbon, and bare soils. Based on our studies thus far conducted, the SWIR2 spectral region continues to stand out as a potential means for providing these needed data.

8. Acknowledgements

We thank B. Sawtelle, C. Cody, and B. Nolen for their invaluable assistance in the field studies presented in this paper. We thank two anonymous reviewers of the manuscript and A. Karnieli for providing editorial guidance. We also thank the personnel from Jornada Long-term Ecological Research program, the USDA Jornada Experimental Range office, and the NASA AVIRIS Program. This work was supported by NASA NIP grant NAG5-8709 and NASA New Millennium (EO-1) Program grant NCC5-480 to G. Asner.

9. References

- ASNER, G.P., 1998, Biophysical and biochemical sources of variability in canopy reflectance, *Remote Sensing of Environment*, 64, 234-253.
- ASNER, G.P., Biophysical remote sensing signatures of arid and semi-arid ecosystems, *Manual of Remote Sensing*, S.L. Ustin ed., John Wiley & Sons, New York, in press.
- ASNER, G.P. and LOBELL, D.B., 2000, A biogeophysical approach for automated SWIR unmixing of soils and vegetation. *Remote Sensing of Environment*, 66, 99-112.
- ASNER, G.P., WESSMAN, C.A., BATESON, C.A., and PRIVETTE, J.L., 2000, Impact of tissue, canopy and landscape factors on reflectance variability of arid ecosystems. *Remote Sensing of Environment*, 66, 69-84.
- BATESON, C.A., ASNER, G.P., and WESSMAN, C.A., 2000, Endmember bundles: A new approach to incorporating endmember variability in spectral mixture analysis, *IEEE Transactions on Geoscience and Remote Sensing*, 38, 1083-1094.
- BATESON, C.A., and CURTISS, B., 1996, A method for manual endmember selection and spectral unmixing. *Remote Sensing of Environment*, 55, 229-243.
- BEN-DOR, E., IRONS, J.R., and EPEMA, G.F., 1999, Soil reflectance, in *Remote Sensing for the Earth Sciences: Manual of Remote Sensing*, A.N. Rencz ed., John Wiley & Sons, New York, pp. 111-188.
- BUFFINGTON, L.C. and HERBEL, C.H., 1965, Vegetation changes on a semidesert grassland range from 1858 to 1963, *Ecological Monographs*, 35, 139-163.
- CARLSON, T.N., and RIPLEY, D.A., 1997, On the relationship between NDVI, fractional vegetation cover, and leaf area index, *Remote Sensing of Environment*, 62, 241-252.

- CLARK, R.N., 1999, Spectroscopy of rocks and minerals, and principles of spectroscopy, in Remote Sensing for the Earth Sciences: Manual of Remote Sensing, A. N. Rencz ed., John Wiley & Sons, New York, pp. 3-58.
- CURRAN, P.J., 1989, Remote sensing of foliar chemistry, Remote Sensing of Environment, 30, 271-278.
- DUNCAN, J., STOW, D., FRANKLIN, J., and HOPE, A., 1993, Assessing the relationship between spectral vegetation indices and shrub cover in the Jornada Basin, New Mexico, International Journal of Remote Sensing, 14, 3395-3416.
- ELMORE, A.J., MUSTARD, J.F., MANNING, S.J., and LOBELL, D.B., 2000, Quantifying vegetation change in semiarid environments, Remote Sensing of Environment, 73, 87-102.
- GAO, B.-C., HEIDEBRECHT, K.B., and GOETZ, A.F.H., 1993, Derivation of scaled surface reflectance from AVIRIS data. Remote Sensing of Environment, 44, 145-163.
- HUETE, A.R., 1988, A soil-adjusted vegetation index (SAVI), Remote Sensing of Environment, 25, 295-309.
- KARNIELI, A., KIDRON, G., GHASSLER, C., and BEN-DOR, E., 1999, Spectral characteristics of cyanobacteria soil crust in the visible, near-infrared, and shortwave infrared (400-2500 nm) in semiarid environment, International Journal of Remote Sensing, 69, 67-77.
- OKIN, G.S., and ROBERTS, D.A., 2000, Linear unmixing of simulated noisy spectra: Vegetation detection limits in areas of low cover, in Proceedings of the 9th JPL Airborne Earth Science Workshop, R.O. Green ed., Jet Propulsion Laboratory, Pasadena, CA.
- RANGO, A., CHOPPING, M., RITCHIE, J., HAVSTAD, K., KUSTAS, W., and SCHMUGGE, T., 2000, Morphological characteristics of shrub coppice dunes in desert grasslands of Southern New Mexico derived from scanning LIDAR, Remote Sensing of Environment, 74, 26-44.
- ROBERTS, D.A., GARDNER, M., and GREEN, R.O., 1998, Mapping chaparral in the Santa Monica Mountains using multiple endmember spectral mixture models, Remote Sensing of Environment, 65, 267-279.
- SCHLESINGER, W.H., and PILMANIS, A.M., 1998, Plant-soil interactions in deserts, Biogeochemistry, 42, 169-184.
- SCHLESINGER, W.H., RAIKES, J.A., and CROSS, A.F., 1996, On the spatial pattern of soil nutrients in desert ecosystems, Ecology, 77, 364-376.
- SCHLESINGER, W.H., REYNOLDS, J. F., CUNNINGHAM, G. L., HUENNEKE, L. F., JARRELL, W.M., VIRGINIA, R.A., and WHITFORD, W.G., 1990, Biological feedbacks in global desertification, Science, 247, 1043-1048.
- SMITH, M.O., USTIN, S.L., ADAMS, J.B., and GILLESPIE, A.R., 1990, Vegetation in deserts: I. A regional measure of abundance from multispectral images, Remote Sensing of Environment, 31, 1-26.
- SOHN, Y., and McCOY, R.M., 1997, Mapping desert shrub rangeland using spectral unmixing and modeling spectral mixtures with TM data, Photogrammetric Engineering and Remote Sensing, 63, 707-716.
- VAN LEEUWEN, W.J.D., and HUETE, A.R., 1996, Effects of standing litter on the biophysical interpretation of plant canopies with spectral indices, Remote Sensing of Environment, 55, 123-138.
- VAN LEEUWEN, W.J.D., HUETE, A.R., WALTHALL, C.L., PRINCE, S.D., BEGUE, A., and ROUJEAN, J.L., 1997, Deconvolution of remotely sensed spectral mixtures for retrieval of LAI, fAPAR and soil brightness, Journal of Hydrology, 188/189, 697-724.

WESSMAN, C.A., BATESON, C.A., and BENNING, T.L., 1997, Detecting fire and grazing patterns in tallgrass prairie using spectral mixture analysis, *Ecological Applications*, 7, 493-512.

WHITE, M.A., ASNER, G.P., NEMANI, R.R., PRIVETTE, J.L., and RUNNING, S.W., 2000, Monitoring fractional cover and leaf area index in arid ecosystems: digital camera, radiation transmittance, and laser altimetry results, *Remote Sensing of Environment*, 74, 45-57.

Table 1. Permutations of AVIRIS data used in Monte Carlo spectral mixture analysis of shrubland and grassland sites. The Landsat TM, MODIS and ASTER satellite instruments were simulated using the AVIRIS data convolved to actual sensor response functions. Special treatment for bad bands and for normalizing various wavelength regions (tying and dividing) are also shown.

Technique/Instrument	Wavelength Region(s)	Special Treatment
AVIRIS	Contiguous 0.4-2.5 μm , 168 channels	Atmospheric water absorption bands (1.3-1.5 μm and 1.8-2.0 μm) are ignored.
AVIRIS VNIR	Contiguous 0.4-1.3 μm , 98 channels	---
AVIRIS SWIR2	Contiguous 2.0-2.3 μm , 45 channels	---
AVIRIS Tied-SWIR2	Contiguous 2.0-2.3 μm , 45 channels	The value at the first wavelength at 2.03 μm is subtracted from the reflectance value at each wavelength.
AVIRIS Divided-SWIR2	Contiguous 2.0-2.3 μm , 45 channels	The reflectance value at each wavelength is divided by value at the first wavelength at 2.03 μm .
Landsat 5 TM	0.48, 0.57, 0.66, 0.84, 1.68, 2.22 μm	---
MODIS	0.41, 0.44, 0.46, 0.49, 0.52, 0.54, 0.55, 0.66, 0.67, 0.74, 0.85, 0.90, 0.93, 0.94, 1.2, 1.6, 2.1 μm	---
ASTER	0.56, 0.66, 0.80, 1.7, 2.16, 2.21, 2.26, 2.33, 2.39 μm	---
ASTER Tied-SWIR2	2.16, 2.21, 2.26, 2.33, 2.39 μm	The value at the first wavelength at 2.16 μm reflectance is subtracted from the value at each wavelength.
ASTER Divided-SWIR2	2.16, 2.21, 2.26, 2.33, 2.39 μm	The reflectance value at each wavelength is divided by value at the first wavelength at 2.16 μm .

Table 2. Summary of estimated photosynthetic vegetation (PV), non-photosynthetic vegetation (NPV), and bare soil cover fractions from 10 different wavelength sampling analyses using *AutoMCU*. Fractional cover results from field measurements are also given. Sums of the three fractions are also shown for each set of estimates.

Permutation		Study Site			
		Shrubland	Std Dev	Grassland [§]	Std Dev
FIELD MEASUREMENTS	PV	0.181*	0.010*	0.069	0.033
	NPV	0.010**	0.010**	0.367	0.133
	Soil	0.820*	0.020*	0.586	0.173
	SUM	1.01	---	1.01	---
AVIRIS Full-range	PV	-0.006	0.060	-0.176	0.036
	NPV	0.019	0.043	0.325	0.031
	Soil	1.053	0.036	0.795	0.036
	SUM	1.06	---	0.94	---
AVIRIS VNIR	PV	0.006	0.044	-0.074	0.028
	NPV	0.147	0.063	0.694	0.066
	Soil	0.953	0.069	0.404	0.078
	SUM	1.11	---	1.02	---
AVIRIS SWIR2 (No tying)	PV	-0.531	0.107	-0.124	0.088
	NPV	0.162	0.042	0.433	0.041
	Soil	1.081	0.035	0.736	0.037
	SUM	0.71	---	1.05	---
AVIRIS Tied SWIR2	PV	0.148	0.062	0.129	0.057
	NPV	0.013	0.034	0.326	0.038
	Soil	0.839	0.050	0.548	0.060
	SUM	1.0	---	1.01	---
AVIRIS Divided SWIR2	PV	0.026	0.011	0.029	0.011
	NPV	0.036	0.020	0.264	0.029
	Soil	0.94	0.016	0.707	0.026
	SUM	1.0	---	1.01	---
Landsat TM	PV	0.375	0.028	0.139	0.030
	NPV	0.242	0.059	0.807	0.062
	Soil	0.836	0.057	0.285	0.285
	SUM	1.45	---	1.23	---
MODIS	PV	-0.049	0.051	-0.222	0.032
	NPV	0.234	0.040	0.570	0.053
	Soil	0.947	0.041	0.642	0.038
	SUM	1.13	---	0.99	---
ASTER Full-range	PV	0.023	0.041	-0.163	0.023
	NPV	-0.002	0.053	0.295	0.046
	Soil	1.066	0.041	0.822	0.031
	SUM	1.09	---	0.95	---
ASTER Tied SWIR2	PV	0.271	0.195	0.271	0.205
	NPV	-0.187	0.172	0.127	0.167
	Soil	0.916	0.068	0.609	0.072
	SUM	1.0	---	1.01	---

* From a combination of IKONOS (Figure 4) - uncertainty values given as ranges and not standard deviations; ** From field observations; [§] From Figure 3.